



Liang, J. et al. (2019) Investigation of Pt-salt-doped-standalone-multiwall carbon nanotubes for on-chip interconnect applications. *IEEE Transactions on Electron Devices*, (doi:[10.1109/TED.2019.2901658](https://doi.org/10.1109/TED.2019.2901658))

This is the author's final accepted version.

There may be differences between this version and the published version. You are advised to consult the publisher's version if you wish to cite from it.

<http://eprints.gla.ac.uk/181807/>

Deposited on: 14 March 2019

Enlighten – Research publications by members of the University of Glasgow
<http://eprints.gla.ac.uk>

Investigation of Pt-Salt Doped Stand-Alone Multi-Wall Carbon Nanotubes for On-Chip Interconnect Applications

Jie Liang, Rongmei Chen, Raphael Ramos, Jaehyun Lee, Hanako Okuno, Dipankar Kalita, Vihar Georgiev, Salim Berrada, Toufik Sadi, Benjamin Uhlig, Katherina Lilienthal, Abitha Dhavamani, Fabian Könemann, Bernd Gotsmann, Goncalves Goncalves, Bingan Chen, Asen Asenov, Jean Dijon, and Aida Todri-Sanial

Abstract—In this paper, we investigate by combining electrical measurements with an atomistic-to-circuit modeling approach, the conductance of doped stand-alone multi-wall carbon nanotubes (MWCNTs) as a viable candidate for the next-generation of back-end-of-line (BEOL) interconnects. Ab-initio simulations predict a doping-related shift of the Fermi level, which reduces shell chirality variability and improves electrical resistivity up to 90% by converting semiconducting shells to metallic. Electrical measurements of Pt-salt doped CNTs provide up to 50% of resistance reduction, which is a milestone result for future CNT interconnect technology. Moreover, we find that defects and contacts introduce additional resistance, which limits the efficiency of doping and are the primary cause for the mismatch between theoretical predictions and experimental measurements on doped CNTs.

Index Terms—Carbon nanotube, defective CNTs, doped CNTs, local on-chip interconnects, individual CNT growth, doping process of CNT, CNT contact resistance.

I. INTRODUCTION

DESIGNING high-performance systems requires fast, dense and high-bandwidth interconnects. In the current back-end-line (BEOL) technology, interconnects are realized by using copper (Cu) with low-k inter-layer dielectric material using dual damascene process. The geometrical dimensions of the trenches and the material used as a conductor determine the resistivity. As the dimensions of Cu wires decrease and become comparable or smaller than its electron mean free path (MFP), size effects such as electron scattering at wire

surface and grain boundaries, and line edge roughness cause the effective resistivity to increase rapidly [1] [2]. Increase in resistivity of Cu lines will unavoidably cause performance degradation as time delay is dominated by resistance and capacitance (R and C).

Atomically thin, ballistic transport, large electron MFP and highly conductive carbon-based materials such as carbon nanotubes (CNTs) provide compelling advantages for the next generation of on-chip interconnects [3], [4]. CNTs are also listed as one of the future materials for advanced technology nodes based on IRDS 2017 report [5]. There are different types of CNTs, single-wall (SW) and multi-wall (MW), according to the number of carbon shells. Different shell rotation indicates the chirality property of shells as either semiconducting or metallic CNTs. Stand-alone metallic CNTs are good candidates for advanced low dimensions interconnect applications [6]. However, individual metallic SWCNT is limited by the intrinsic quantum resistance ($\sim 6.45 \text{ k}\Omega$) [7], [8] for lengths longer than its MFP, hence the total resistance further increases with phonon scattering [9]. Moreover, using a single shell as interconnect is prone to connections issues during the fabrication process, defects, and highly resistive contacts, thus, overall they can be less reliable. Consequently, multi-wall CNTs (MWCNT) with numerous parallel shells are considered to enhance the CNT conductivity by increasing the number of possible conducting paths. For interconnect applications, it is essential that shells are metallic to obtain high conductivity, hence, raises the importance of MWCNT chirality control.

Doping of MWCNT can be a suitable solution to overcome the random shell chirality. By introducing extrinsic electron sub-bands, hence shifting of Fermi-level, MWCNT semiconducting shells can adopt metallic-like behavior, therefore improving the shell chirality control and enhancing the MWCNT conductivity. In this work, we study both theoretically and experimentally charge-based doping of MWCNTs with Pt-salt as local interconnects. We investigate MWCNT defects and contact resistance to explain the difference between theoretical prediction and experimental measurements. We find that doping is a viable solution to enhance CNT conductivity and control chirality variation, and even alleviate some of the undesirable impacts of defects and high contact resistance.

This work was supported by the European Commission H2020 CONNECT project under grant agreement number 688612. (<http://www.connect-h2020.eu/>).

J. Liang, R. Chen and A. Todri-Sanial are with the Microelectronics Department, LIRMM, University of Montpellier, CNRS, Montpellier, 34095 France. E-mail: aida.todri@lirmm.fr.

R. Ramos, and J. Dijon are with the University Grenoble Alpes/CEA-LITEN, Grenoble, France.

J. Lee, S. Berrada, V. Georgiev, and A. Asenov are with the School of Engineering, University of Glasgow, Glasgow, G12 8QQ UK.

H. Okuno and D. Kalita are with the University Grenoble Alpes/CEA-INAC, Grenoble, France.

B. Uhlig, K. Lilienthal and A. Dhavamani are with the Fraunhofer IPMS, Dresden, Germany.

F. Könemann and B. Gotsmann are with the IBM Research Zurich, Switzerland.

G. Goncalves and B. Chen are with the Aixtron Ltd., Cambridge, UK.

T. Sadi is with the School of Engineering, University of Glasgow, Glasgow, G12 8QQ UK and the Aalto University, Finland.

Manuscript submitted August 2018.

II. ELECTRICAL COMPACT MODELS

CNT interconnect electrical models have already been established by [10] and [11] where pristine SWCNTs and MWCNTs for on-chip interconnects were investigated. In contrast to these works, we consider modeling of charge-based doped MWCNT interconnects. We perform both atomistic- and circuit-level simulation to understand the impact of doping on Fermi-level shift and MWCNT parasitics.

A. Doping of MWCNT

Doping of CNTs with electron donor (n-type)/acceptor (p-type) presents a practical solution to overcome variations on random chirality and shell variability in MWCNTs. Doping shifts the material Fermi-Level, thus enhancing metallic properties for semiconducting tubes and reducing the metallic tube resistivity by introducing additional electron transport channels. Comparing to substitutional doping in CNTs which forms a Bamboo-like morphological deformation [12], we investigate, in this work, charge transfer doping as a viable method to control MWCNT chirality. In the charge transfer doping, dopants do not form covalent bonds, but rather Van der Waals interactions take place, hence there is no structural modification. Due to interactions with the ambient environment, pristine CNTs behave lightly p-type doped [13], hence introducing a p-type dopant is practically more feasible. There exists various kinds of p-type dopant such as NO_2 [14], H_2SO_4 and SOCl_2 [15], and the combination of HNO_3 and SOCl_2 [16], etc. [17]. Recently, iodine [18], MoO_3 [19] and PtCl_4 [20], [21] based p-type charge transfer doping have been presented. In this paper, our models are based on PtCl_4 charge transfer p-type doping.

B. Atomistic model - DFT Calculation

We have performed the Density Functional Theory (DFT) simulations, which is implemented in the Atomistix Tool Kit (ATK) [22] to investigate the electrical properties of Pt-salt doped CNTs. The generalized gradient approximation (GGA) is applied to the exchange-correlation energy function. We have compared the formation energies with atomic structures using PtCl_4 as a dopant agent inside and outside the CNT. When PtCl_4 is located inside the CNT, the structure is most stable. Fig. 1 (a) shows the band structure and density-of-states (DOS) of pristine and doped metallic CNT (15,0). We have found that Pt-salt is a good p-type dopant. Thanks to the Fermi-level (E_F) shift, the doped CNT has a larger DOS near E_F . The band structure and DOS of the semiconductor CNT (16,0) are shown in Fig. 1 (b). Due to E_F shift, the semiconductor CNT can have a metallic behavior. The value of E_F shifts in double-wall CNTs (DWCNTs) is also calculated, and we notice that inner shell of CNT is also impacted by doping with similar Fermi-shift. To summarize, doping of CNTs reduces the chirality variability of shells by degenerating semiconducting shells, which acquire metallic properties.

C. Electrical RC model

Each MWCNT shell has a different number of conducting channels due to shell chirality and diameter. we introduce N_c

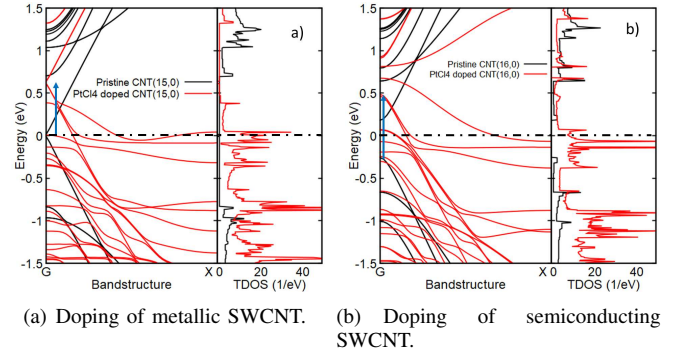


Fig. 1: Band structure and total DOS of pristine and PtCl_4 doped (a) CNT (15,0) (See Fig 1. b)). Fermi-level (E_F) is set to 0.0 eV. Due to the dopant, E_F is shifted by -0.6 eV, and DOS near E_F has increased. (b) CNT (16,0). E_F shifts by dopants, semiconductor CNT (16,0) has become a metal.

to represent the number of conducting channels per shell and as a parameter for controlling chirality variability knowing that doping alters semiconducting shells to acquire metallic properties. The number of conducting channels per shell is theoretically expressed in [23]. With doping, shifting of E_F can tune the energy distance to the occupied sub-bands, thus further increase the probability of electrons to contribute to electrical transport, hence more conducting channels are available with doping of CNTs. From analytical computations of N_c [23], we assume a pristine metallic shell with a diameter less than 10nm has two conducting channels, $N_c = 2$. After doping, when a semiconducting shell acquires a $N_c \geq 2$, we interpret such increase of conducting channels as a conversion of shell property from semiconducting to metallic [24].

For a single conducting channel, its conductance is derived as:

$$G_{1channel} = G_0 / (1 + L/L_{MFP}) \quad (1)$$

where G_0 is the quantum conductance ($\sim 1/12.9 \text{ k}\Omega$) and L_{MFP} is the CNT electron mean free path. CNT mean free path depends on the CNT diameter and a derivation of CNT mean free path is provided in [11] as:

$$L_{MFP} \approx 1000 D_{MWCNT} \quad (2)$$

Hence, the total doped MWCNT resistance R_{MWCNT} is derived as:

$$R_{MWCNT} = \frac{1}{N_c N_s G_{1channel}} \quad (3)$$

where N_s is the number of shells and is derived as *diameter-1* based on experimental statistical measurements [25].

CNT has quantum (C_Q) and electrostatic capacitance (C_E) [11]. C_Q depends on N_c and N_s , as the CNT quantum capacitance refers to the capability of storing electron energy [26]. Doped MWCNT total quantum capacitance is derived as:

$$C_Q = N_c N_s C_{Q/channel} \quad (4)$$

In Fig. 2, we show the resistivity of 7 nm diameter MWCNT with lengths up to $10 \mu\text{m}$ while varying N_c . We compare the

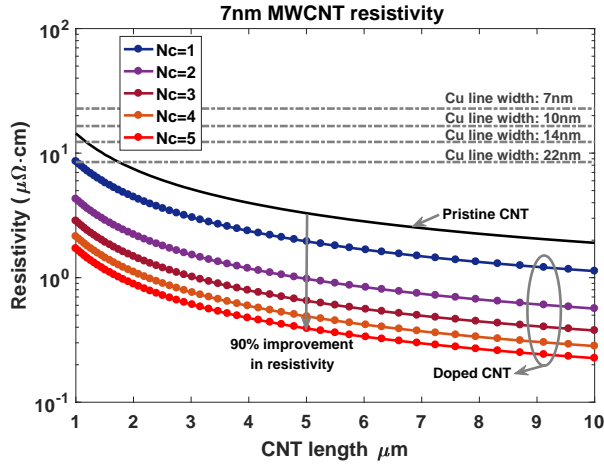


Fig. 2: 7nm diameter MWCNT resistivity with different doping levels where the increase of N_c indicates more doping concentration.

resistivity of copper (Cu) lines with line widths of 22, 14, 10 and 7 nm [33]. We observe that doping improves CNT resistivity and achieves even lower resistivity than pristine CNTs and Cu lines. We notice that resistivity of pristine CNTs becomes advantageous to Cu lines for lengths beyond $2 \mu\text{m}$. With doping, CNT resistivity improves even shorter lengths, which prompts further investigation of doped CNTs for local short on-chip interconnects where Cu line performance significantly degrades with scattering. We obtain up to 90% improvement in resistivity of ideal CNTs without considering contacts by doping of $N_c=5$.

However, using CNTs for local on-chip interconnects has to consider the contact resistance and CNTs quality where defects are often existing to degrade CNTs performance. When MWCNTs are grown in low-temperature ($\sim 600^\circ\text{C}$) CVD, it is challenging to obtain high-quality CNTs. Various types of defects can be introduced during the growth process, [27], [28], which result in shortening the ballistic transport (or electron mean free path). The reduction in mean free path leads to higher MWCNT resistance [29]. Additionally, the contact between metal and CNTs can be of considerable resistance. There are commonly two types of contacts, end-contact [30] and side-contacts [31]. We introduce two fitting parameters to our MWCNT model: defect-related mean free path [32] and contact resistance, R_c as:

$$L_{MFP}^D \approx \alpha \cdot D_{MWCNT} \quad (5)$$

$$\begin{aligned} R_{MWCNT}^D &= \frac{1}{N_c N_s G_{1channel}} + 2R_c \\ &= \frac{1 + L/L_{MFP}^D}{N_c N_s G_0} + 2R_c \end{aligned} \quad (6)$$

where Eq. 5 represents the mean free path with defects. Low values of α represent short mean free path and a highly defective CNT. Eq. 6 represents the defective MWCNT resistance together with contact resistances. These equations

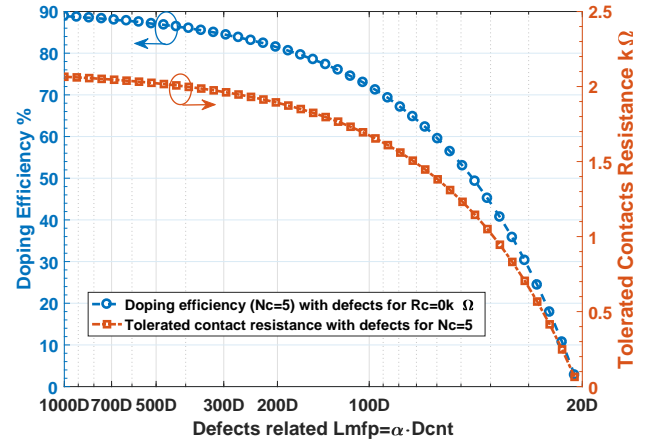


Fig. 3: For MWCNT of diameter 7nm, it is shown in the left Y-axis that doping efficiency of $N_c=5$ varies with defects and no contact resistance. With doping of $N_c=5$, tolerated contact resistance to remain the total resistance unchanged for various defect scenarios is shown in the right Y-axis. Each tolerated contact resistance is derived with corresponding doping efficiency for each defect scenario.

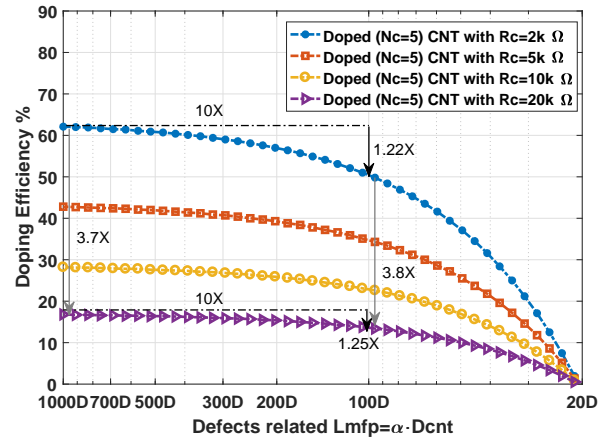


Fig. 4: Doping efficiency of MWCNT of diameter 7nm. Doping concentration is fixed as $N_c=5$. The presence of contact resistance decreases the doping efficiency for various defects concentration.

indicate that MWCNT resistance increases with defects (or decrease of mean free path L_{MFP}^D) and contact resistance, R_c . When doping is applied, the number of conducting channels N_c increases which helps to reduce MWCNT resistance and alleviate some of the detrimental impacts of defects.

We update our model to include different mean free paths. The term $L_{MFP}^D = \alpha \cdot D_{MWCNT}$ represents different defects densities due to the change in the mean free path where the smaller α is, the higher the defect density and shorter the electron mean free path become. $L_{MFP} = 1000D_{MWCNT}$ represents the defect-free MWCNT [11]. In Fig. 3, we show the doping efficiency for a 7nm doped ($N_c=5$) MWCNT without contact resistance to pristine MWCNT. We compute

doping efficiency (i.e. improvement in MWCNT resistance with doping) as a function of defects on the x-axis. Overall, doping helps to improve MWCNT resistance as shown in the left y-axis. But, we note a decrease in doping efficiency with the increase in defect density, as defects worsen CNT total resistance. For each defect density, we also compute the tolerated contact resistance due to the improvement of MWCNT resistance from doping. Thus, as doping helps to improve the MWCNT resistance, it indirectly also allows tolerating contact resistance without changing the total pristine MWCNT resistance (Eq. 6). Both doping efficiency and tolerated contacts drastically decrease when the CNT is highly defective ($L_{MFP} \sim 20D_{MWCNT}$).

So far, we have studied CNTs stand-alone without considering the contact resistance as in a realistic BEOL structure. In Fig. 4 we show doping efficiency for different kinds of contacts such as side-/end-contacts and different metals. Doping efficiency compares doped ($N_c=5$) MWCNT to pristine MWCNT under various contacts and as a function of defects. To represent a wide range of contact resistance values, we consider $R_c=2k\Omega$ to $R_c=20k\Omega$. First, we notice that contact resistances reduce doping efficiency and in conjunction with defects their combined effect is detrimental for doping. For example, a pristine CNT with $L_{MFP} = 1000D_{MWCNT}$ undergoes a reduction of 3.7X in doping efficiency when contacts increase 10X from $2k\Omega$ to $20k\Omega$. But for a 10X increase in defect density (i.e. mean free path from $1000D$ to $100D$), doping efficiency undergoes a reduction of 1.22X and 1.25X for contact resistance of $2k\Omega$ and $20k\Omega$, respectively. Thus, contact resistances are predominant compared to defects and they both reduce doping efficiency.

III. EXPERIMENTAL DOPING PROCESS AND MEASUREMENTS

Here, we describe the process of chemical vapor deposition (CVD) grown CNTs in relatively low temperatures ($\sim 600^\circ C$) for on-chip interconnect applications and compatible with CMOS BEOL process line. $PtCl_4$ charge based doping process is developed, and CNT/Palladium side contacts are realized for electrical characterization.

A. CNT Growth

CNT growth is achieved by hot filament assisted catalytic chemical vapor deposition (CVD) using iron catalyst and acetylene carbon precursor at a temperature around $600^\circ C$. To ensure controlled placement of CNT, the catalyst is localized at the bottom of via holes prepared by standard nano-fabrication technology (Fig. 5). We developed a unique method to grow individual small diameter MWCNT with controlled structure. This relies on the formation of a single catalyst droplet - hence a single CNT - in the via hole during CVD growth. It is achieved by precisely tuning the quantity of catalyst, the nature of the catalyst support and CNT growth parameters. Typically, the growth of individual MWCNT can be realized on aluminosilicate support with 1 nm thick iron catalyst if the hole diameter is less than 40 nm (Fig. 5). Fig. 6 displays TEM images of individual CNTs grown from via holes with a

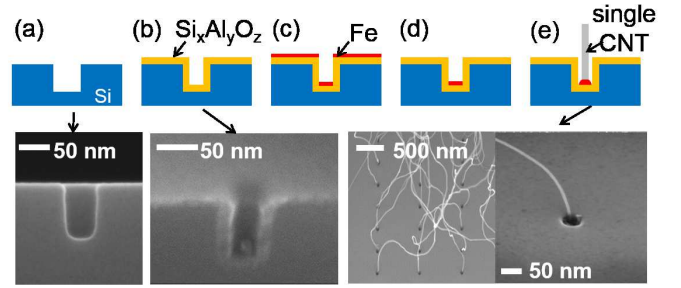


Fig. 5: Localized growth of a single MWCNT from a via hole. (a) Via hole prepared in silicon substrate by E-beam lithography and plasma etching. (b) Conformal deposition of aluminosilicate by atomic layer deposition to trim the hole diameter. (c) Directional E-beam evaporation of 1 nm Fe catalyst at normal incidence. (d) Ion beam etching of top surface catalyst at grazing incidence. (e) CNT growth by hot filament CVD.

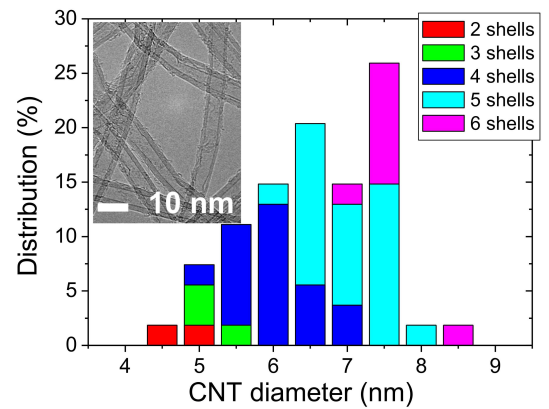


Fig. 6: Statistical distribution of the diameter and number of shells of individually grown CNTs from 30 ± 10 nm diameter via hole with representative TEM image (inset). Median CNT diameter is 6.5 ± 1 nm with 4 - 5 shells.

diameter of 30 ± 10 nm. It also shows the distribution of CNT diameter ($6.5 \text{ nm} \pm 1 \text{ nm}$) and the number of shells (mostly 4 and 5 walls). CNTs grown on 300 mm wafers are processed using AIXTRON BM 300T system. The CNT growth occurs in a cold wall reactor using a vertical gas flow distributed via a showerhead. This configuration allows a fast scaling of the process conditions from the coupon size to the 300 mm wafer scale.

B. $PtCl_4$ Doping Process

We considered both external and internal doping of CNTs by charge transfer from $PtCl_4$. For external doping, the MWCNTs are dipped into $PtCl_4$ solution. For internal doping, a structural opening of the tip of CNT is necessary for effective internal doping of CNTs. It allows for the dopants to enter the inner tubes of the CNT and remain confined. We find that CNTs treated with an oxygen plasma under mild conditions ensure high CNT filling rate of 30%. This filling rate is not absolute but could vary with $PtCl_4$ concentration and density of CNTs. Figure 7 (a) shows the HAADF-TEM image of

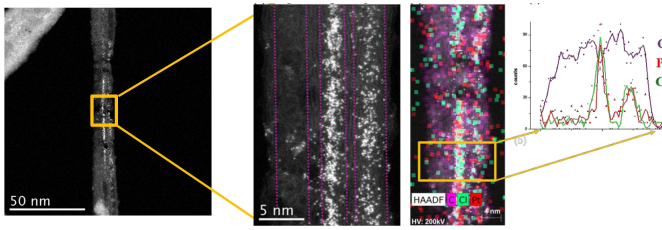


Fig. 7: (a) HAADF-TEM image of CNTs with different concentration of dopant (purple dotted lines shows the different CNTs). (b) EDX mapping of Pt-Cl doped CNTs. (c) Line scan of EDX mapping across doped CNT. Purple, red, green color represents Carbon, Platinum and Chlorine respectively.

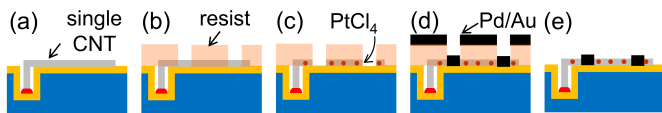


Fig. 8: Process flow for internally-doped end-contacted single CNT interconnect line. (a) Single CNT grown from via hole and flipped down on the surface. (b) Photolithography to pattern the contact pads. (c) Plasma etching of CNT followed by dipping in $PtCl_4$ solution to introduce dopant inside the CNT. (d) Physical vapor deposition of Pd/Au contact metal stack. (e) Contact pad fabrication by lift-off. The same process flow is used to fabricate side-contacted CNT interconnect by suppressing step (c). External doping of CNT is achieved by dipping the sample after step (e) in the dopant solution.

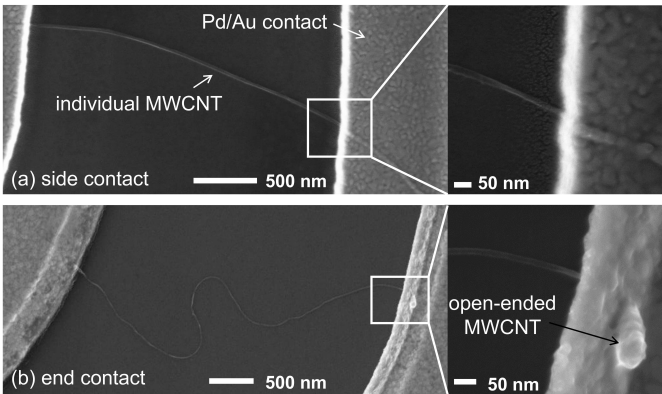
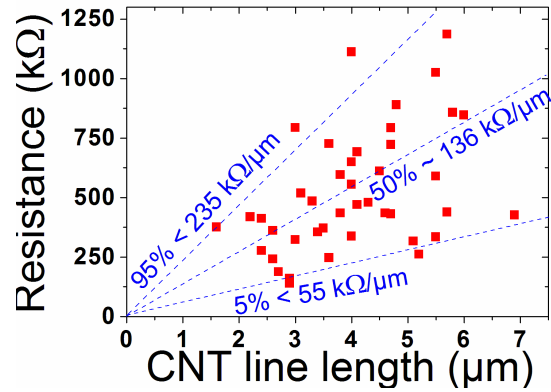
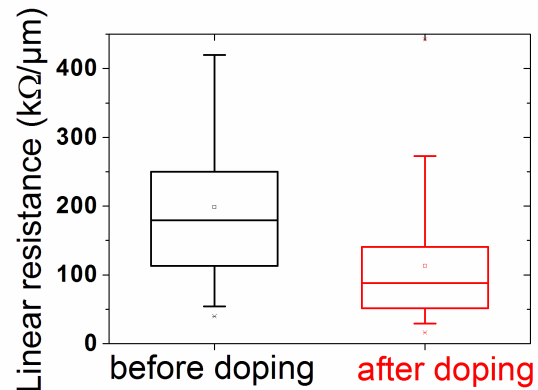


Fig. 9: SEM images of electrically connected individual MWCNT with (a) side and (b) end contacts made out of Pd (40nm) and Au (150nm).

the CNT opened with oxygen plasma process and doped with Pt-Cl network of dopants. The three different CNTs are highlighted with doped dotted purple lines. The Pt and Cl elements within the doped-CNT were verified using Energy-Dispersive X-ray spectroscopy (EDX) mapping shown in Fig. 7 (c). The difference in concentration between neighboring CNTs is due to partial amorphization induced by plasma treatment. Based on these results, a dedicated process flow for contact fabrication and doping of integrated CNT was developed (Fig. 8). Both side-contact and end-contact were



(a) Electrical resistance measurement before doping.



(b) Before vs. after doping.

Fig. 10: (a) Two points probe resistance measurement for a collection of individual CNTs before doping. (b) 50% improvement of linear resistance with external $PtCl_4$ doping.

realized on individual MWCNT (Fig. 9).

C. Electrical Measurements

A set of individual MWCNT interconnect fabricated in parallel on the same sample was electrically characterized. The CNTs were grown from 30 ± 10 nm diameter via holes and side-contacted with Pd according to the process flow in Fig. 8 (omitting step (c)). Two-point-probe current-voltage characteristics were systematically recorded to extract the electrical resistance (CNT resistance + CNT/Pd side contact resistance). Fig. 10 (a) displays the measured resistance as a function of the CNT length. It is observed that resistance increases with CNT length in the 1-10 μm range, which is expected for diffusive transport in CVD-grown, hence, defective CNTs. However, a large scatter in the data is observed, thus revealing variability in MWCNT conductivity and contact resistance. The origin of the variability may be the variability in the diameter, the number of shells of each CNT (cf Fig. 6), the random repartition of metallic versus semiconducting shells, the presence of defects, or variability in the contact fabrication technology. Assuming the measured resistance is dominated by the resistivity of MWCNT, linear resistance is spread between

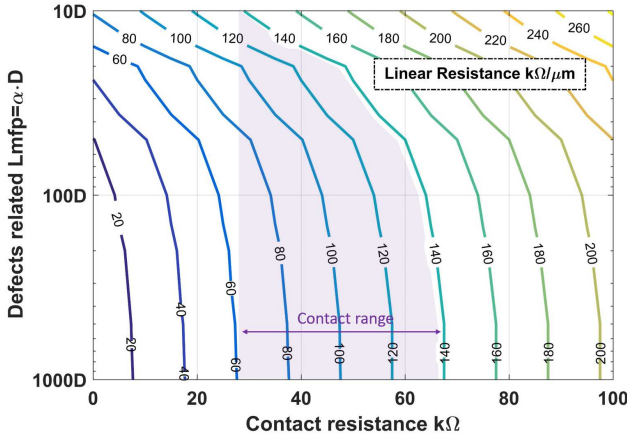


Fig. 11: Theoretical prediction of linear resistance for a defective pristine MWCNT with contact resistances, similar conditions to the experimental measurements. 1000D means defects free and 10D represents highly defective.

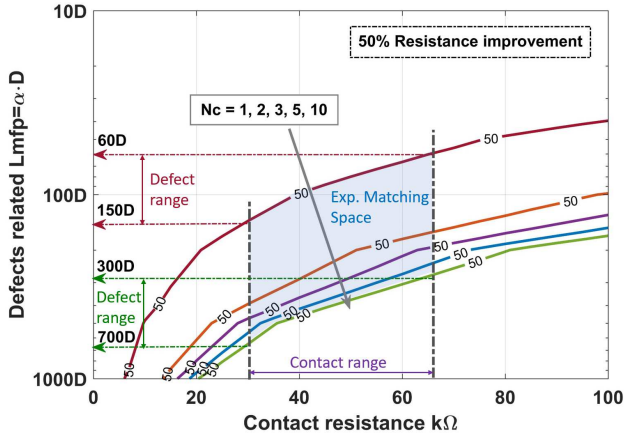


Fig. 12: 50% of resistance improvement after doping with different N_c (red line: $N_c=1$; green line: $N_c=10$). Resistance improvement has also dependence on contact resistance and defects related CNT mean free path. 1000D means defects free and 10D represents highly defective.

55 and 235 $k\Omega/\mu m$ (90% envelope). Preliminary electrical results of doped CNTs by $PtCl_4$ were obtained by using external doping of side-contacted single CNT interconnects. Fig. 10 (b) displays the measured linear resistance (resistance divided by CNT length) for the same set of CNTs before and after external doping. It is observed that, on average, the resistance of externally doped MWCNTs is reduced up to 50%. The scatter of data is also reduced, which suggests variability improves with doping.

IV. EXPERIMENTAL VS. SIMULATION RESULTS

From experimental measurements, we obtained a distribution of linear resistances of undoped MWCNTs centered at 136 $k\Omega/\mu m$ with 50% of linear resistance improvement with $PtCl_4$ doping (Fig. 10 (a) and (b)). We suspect that both

defects and contact resistance play an important role on the measured doping efficiency. To understand the reason behind the 50% doping efficiency, we perform variability simulations taking into account the defects and contact resistances as shown in Fig. 11. We plot the linear resistance ($k\Omega/\mu m$) while varying both contacts and defects. For the linear resistance of 136 $k\Omega/\mu m$ (as in experimental results), we identify the range of contact resistances of 30 $k\Omega$ to 67 $k\Omega$ for various defect densities.

To decorrelate the impact of contacts from defects, we investigate various doping levels (such as N_c varying from 1 to 10) to reproduce the 50% doping efficiency from experimental results. The goal is to extract the possible ranges of contact resistances and quality of CVD grown MWCNTs (defect density) such that we can reproduce the experimental results and emulate the experimental impact of doping. In Fig. 12, the 50% resistance improvements curves are shown for various contact resistances and defect densities. We notice that doping from $N_c=5$ to $N_c=10$ has less impact than doping from $N_c=1$ to $N_c=2$. We apply the contact resistance range from 30 $k\Omega$ to 67 $k\Omega$ obtained from Fig. 11 and derive the defect density (or mean free path) in the range of 60D to 150D for light doping of $N_c=1$ or range of 300D to 700D for heavy doping of L_{MFP} . Hence, we extract that the measured 50% doping efficiency can be obtained from the combination of large contact resistance and presence of defects. As the average linear resistance of 136 $k\Omega/\mu m$ and 50% of linear resistance improvement, our MWCNTs have relatively high contact resistance (30 $k\Omega$ to 67 $k\Omega$) and defects related CNT mean free path that vary from 60D to 700D. The possible solution space of doped MWCNTs that exhibit such properties that match experimental results is also highlighted in Fig. 12. Further, four points and six points measurements should be investigated to fully decorrelate the relationship among doping efficiency, contact resistance and defects for standalone MWCNT interconnects. Doping can be a favourable solution to reduce the variability of CNTs and mitigate the drawbacks of contact resistance and defects for CNT interconnect technology. However, beyond doping we still need more investigations on growing better quality CNTs and improving BEOL integration process.

V. CONCLUSION

In this paper, we investigate Pt-salt doped CNT for BEOL interconnects. By combining atomistic to circuit-level simulation and measurement results, we explain the impact of doping on enhancing MWCNT metallic properties. Both experimental data and simulations show that the $PtCl_4$ represents an efficient doping strategy to reduce MWCNT resistivity through conversion of semiconducting shells to metallic ones. Doping can also be a likely solution to overcome the detrimental impacts of defects and contact resistances for a realistic interconnect system. We notice that both contacts and defects reduce doping efficiency and contact resistance is more dominant than defects. This represents a milestone result, which could enable the success of MWCNTs as a candidate for future back-end-of-line technology nodes interconnects.

ACKNOWLEDGMENT

Authors would like to acknowledge H2020 CONNECT European project. This project has received funding from the European Union's Horizon 2020 research and innovation program under grant agreement No 688612. (<http://www.connect-h2020.eu/>). R. R. and J. D. would like to acknowledge Intel Oregon for financial support on CNT TEM characterization.

REFERENCES

- [1] S. Im, N. Srivastava, K. Banerjee, and K. E. Goodson, "Scaling analysis of multilevel interconnect temperatures for high-performance ics," *IEEE Transactions on Electron Devices*, vol. 52, no. 12, pp. 2710–2719, 2005. DOI: 10.1109/TED.2005.859612
- [2] W. Steinhögl, G. Schindler, G. Steinlesberger, M. Traving, and M. Engelhardt, "Comprehensive study of the resistivity of copper wires with lateral dimensions of 100 nm and smaller," *Journal of Applied Physics*, vol. 97, no. 2, p. 023706, 2005. DOI: 10.1063/1.1834982
- [3] A. Todri-Sanial, J. Dijon, and A. Maffucci, *Carbon Nanotubes for Interconnects*. Springer, 2017 ISBN: 978-3-319-29744-6.
- [4] A. Todri-Sanial, R. Ramos, H. Okuno, J. Dijon, A. Dhavamani, M. Widlicenus, K. Lilienthal, B. Uhlig, T. Sadi, V. Georgiev *et al.*, "A survey of carbon nanotube interconnects for energy efficient integrated circuits," *IEEE Circuits and Systems Magazine*, vol. 17, no. 2, pp. 47–62, 2017. DOI: 10.1109/MCAS.2017.2689538
- [5] (2017) international roadmap for devices and systems. [Online]. Available: <https://irds.ieee.org/roadmap-2017>
- [6] G. F. Close, S. Yasuda, B. Paul, S. Fujita, and H.-S. P. Wong, "A 1 ghz integrated circuit with carbon nanotube interconnects and silicon transistors," *Nano Letters*, vol. 8, no. 2, pp. 706–709, 2008. DOI: 10.1021/nl0730965
- [7] S. Frank, P. Poncharal, Z. Wang, and W. A. De Heer, "Carbon nanotube quantum resistors," *science*, vol. 280, no. 5370, pp. 1744–1746, 1998. DOI: 10.1126/science.280.5370.1744
- [8] C. T. White and T. N. Todorov, "Carbon nanotubes as long ballistic conductors," *Nature*, vol. 393, no. 6682, p. 240, 1998. DOI: 10.1038/30420
- [9] P. L. McEuen, M. S. Fuhrer, and H. Park, "Single-walled carbon nanotube electronics," *IEEE transactions on nanotechnology*, vol. 99, no. 1, pp. 78–85, 2002. DOI: 10.1109/TNANO.2002.1005429
- [10] N. Srivastava and K. Banerjee, "Performance analysis of carbon nanotube interconnects for vlsi applications," *IEEE/ACM International conference on Computer-aided design*, pp. 383–390, 2005. DOI: 10.1109/ICCAD.2005.1560098
- [11] H. Li, W.-Y. Yin, K. Banerjee, and J.-F. Mao, "Circuit modeling and performance analysis of multi-walled carbon nanotube interconnects," *IEEE Transactions on electron devices*, vol. 55, no. 6, pp. 1328–1337, 2008. DOI: 10.1109/TED.2008.922855
- [12] B. Padya, D. Kalita, P. Jain, G. Padmanabham, M. Ravi, and K. Bhat, "Self-organized growth of bamboo-like carbon nanotube arrays for field emission properties," *Applied Nanoscience*, vol. 2, no. 3, pp. 253–259, 2012. DOI: 10.1007/s13204-012-0102-z
- [13] P. G. Collins, K. Bradley, M. Ishigami, and d. A. Zettl, "Extreme oxygen sensitivity of electronic properties of carbon nanotubes," *science*, vol. 287, no. 5459, pp. 1801–1804, 2000. DOI: 10.1126/science.287.5459.1801
- [14] J. Kong, N. R. Franklin, C. Zhou, M. G. Chapline, S. Peng, K. Cho, and H. Dai, "Nanotube molecular wires as chemical sensors," *science*, vol. 287, no. 5453, pp. 622–625, 2000. DOI: 10.1126/science.287.5453.622
- [15] V. Skakalova, A. Kaiser, U. Dettlaff-Weglikowska, K. Hrnčarikova, and S. Roth, "Effect of chemical treatment on electrical conductivity, infrared absorption, and raman spectra of single-walled carbon nanotubes," *The Journal of Physical Chemistry B*, vol. 109, no. 15, pp. 7174–7181, 2005. DOI: 10.1021/jp044741o
- [16] B. B. Parekh, G. Fanchini, G. Eda, and M. Chhowalla, "Improved conductivity of transparent single-wall carbon nanotube thin films via stable postdeposition functionalization," *Applied Physics Letters*, vol. 90, no. 12, p. 121913, 2007. DOI: 10.1063/1.2715027
- [17] L. Yu, C. Shearer, and J. Shapter, "Recent development of carbon nanotube transparent conductive films," *Chemical reviews*, vol. 116, no. 22, pp. 13 413–13 453, 2016. DOI: 10.1021/acs.chemrev.6b00179
- [18] Y. Zhao, J. Wei, R. Vajtai, P. M. Ajayan, and E. V. Barrera, "Iodine doped carbon nanotube cables exceeding specific electrical conductivity of metals," *Scientific reports*, vol. 1, p. 83, 2011. DOI: 10.1038/srep00083
- [19] S. Esconjauregui, L. D'Arsié, Y. Guo, J. Yang, H. Sugime, S. Caneva, C. Cepek, and J. Robertson, "Efficient transfer doping of carbon nanotube forests by moo₃," *ACS nano*, vol. 9, no. 10, pp. 10422–10430, 2015. DOI: 10.1021/acsnano.5b04644
- [20] J. Dijon, R. Ramos, A. Fournier, H. Le Poche, H. Fournier, H. Okuno, and J. Simonato, "Record resistivity of in-situ grown horizontal carbon nanotube interconnect," *Technical proceedings of the 2014 NSTI nanotechnology conference and expo, NSTI-Nanotech*, vol. 3, pp. 17–20, 2014. ISBN: 978-1-4822-5830-1
- [21] J. Liang, R. Ramos *et al.*, "A physics-based investigation of pt-salt doped carbon nanotubes for local interconnects," *accepted in IEEE International Electron Devices Meeting (IEDM)*, 2017. DOI: 10.1109/IEDM.2017.8268502
- [22] Atomistix toolkit version 2016.4, quantumwise a/s. [Online]. Available: www.quantumwise.com
- [23] H. Li, W. Lu, J. Li, X. Bai, and C. Gu, "Multichannel ballistic transport in multiwall carbon nanotubes," *Physical review letters*, vol. 95, no. 8, p. 086601, 2005. DOI: 10.1103/physrevlett.95.086601
- [24] R. Chen, J. Liang, J. Lee, V. P. Georgiev, R. Ramos, H. Okuno, D. Kalita, Y. Cheng, L. Zhang, R. R. Pandey *et al.*, "Variability study of mwcnt local interconnects considering defects and contact resistances—part ii: Impact of charge transfer doping," *IEEE Transactions on Electron Devices*, no. 99, pp. 1–8, 2018. DOI: 10.1109/TED.2018.2868424
- [25] N. Chiodarelli, O. Richard, H. Bender, M. Heyns, S. De Gendt, G. Groeseneken, and P. M. Vereecken, "Correlation between number of walls and diameter in multiwall carbon nanotubes grown by chemical vapor deposition," *Carbon*, vol. 50, no. 5, pp. 1748–1752, 2012. DOI: 10.1016/j.carbon.2011.12.020
- [26] P. J. Burke, "Luttinger liquid theory as a model of the gigahertz electrical properties of carbon nanotubes," *IEEE Transactions on Nanotechnology*, vol. 99, no. 3, pp. 129–144, 2002. DOI: 10.1109/tnano.2002.806823
- [27] P. G. Collins, *Defects and disorder in carbon nanotubes*. Oxford University Press Oxford, 2009, pp. 156–184. DOI: 10.1093/oxfordhb/9780199533053.013.2
- [28] M. Zhang and J. Li, "Carbon nanotube in different shapes," *Materials today*, vol. 12, no. 6, pp. 12–18, 2009. DOI: 10.1016/s1369-7021(09)70176-2
- [29] M. Bockrath, W. Liang, D. Bozovic, J. H. Hafner, C. M. Lieber, M. Tinkham, and H. Park, "Resonant electron scattering by defects in single-walled carbon nanotubes," *Science*, vol. 291, no. 5502, pp. 283–285, 2001. DOI: 10.1126/science.291.5502.283
- [30] C. Chen, W. Zhang, L. Wei, Y. Su, N. Hu, Y. Wang, Y. Li, H. Zhong, Y. Liu, X. Liu *et al.*, "Investigation on nanotube-metal contacts under different contact types," *Materials Letters*, vol. 145, pp. 95–98, 2015. DOI: 10.1103/physrevlett.114.085501
- [31] A. D. Franklin and Z. Chen, "Length scaling of carbon nanotube transistors," *Nature nanotechnology*, vol. 5, no. 12, p. 858, 2010. DOI: 10.1038/nnano.2010.220
- [32] M. H. van der Veen, Y. Barbarin, Y. Kashiwagi, and Z. Tokei, "Electron mean-free path for cnt in vertical interconnects approaches cu," pp. 181–184, 2014. DOI: 10.1109/IITC.2014.6831865
- [33] N. C. Wang, S. Sinha, B. Cline, C. D. English, G. Yeric, and E. Pop, "Replacing copper interconnects with graphene at a 7-nm node," pp. 1–3, 2017. DOI: 10.1109/IITC-AMC.2017.7968949